Ultrathin epitaxial Bi film growth on 2D $HfTe_2$ template

Evangelia Xenogiannopoulou[1], Dimitra Tsoutsou[1], Polychronis Tsipas[1], Sotirios Fragkos[1,2], Stefanos Chaitoglou[1], Nikolaos Kelaidis[1] and Athanasios Dimoulas[1]

[1] Institute of Nanoscience and Nanotechnology, National Center for Scientific Research 'Demokritos', 15310, Athens, Greece.
[2] Department of Mechanical Engineering, University of West Attica, 12244, Athens, Greece.

E-mail: e.xenogiannopoulou@inn.demokritos.gr

Received xxxxxx
Accepted for publication xxxxxx
Published xxxxxx

Abstract

Among ultrathin Monoelemental 2D Materials (ME2DMs), bismuthene, the single layer of heavier group-VA element bismuth (Bi), has been predicted to have large nontrivial gap. Here, we demonstrate the growth of 3BL thin Bi(111) films by molecular beam epitaxy (MBE) on 2D-$HfTe_2$ template. The electronic band structure of 3BL Bi(111) films was measured by Angle-Resolved Photoemission Spectroscopy (ARPES) showing very good matching with the theoretical DFT calculated band structure of the respective free standings Bi(111) layers. After capping with protective Al_2O_3 layer, the 3BL thin Bi(111) films on 2D-$HfTe_2$ template were found to be stable under ambient conditions, which is required for practical applications and devices fabrications.

Keywords: term, term, term

1. Introduction

2D TIs are solid state materials that have both an insulating electronic structure in the bulk and dissipation-less conducting channels along the edges that are protected against back-scattering by time-reversal symmetry [1]. The TIs are closely related to the quantum spin Hall (QSH) state, which also has unique edge states, since in these materials the spin-orbit coupling (SOC) takes the role of the applied magnetic field. In TIs, the SOC is so strong that the spin is "locked" perpendicular to the momentum yielding boundary metallic states robust against disorder, scattering or any other excitation [2].

Following the first experimental realization of graphene, other ultrathin Monoelemental 2D Materials (ME2DMs) with novel electronic properties have been explored over the last years [3]. In particular, the two-dimensional (2D) Xenes [4], where X stands for the heavier elements of group IV, single-element sp^2-hybridized silicene [5], germanene [6], stanene [7] and phosphorene [8] were successfully synthesized [9], while the application of silicene was demonstrated in field-effect transistors operating at room temperature (RT) [10]. Within the framework of topological matter, particular attention should be also given to the heavier group-VA element bismuth (Bi), since ultrathin Bi films exhibit a number of interesting properties such as strong SOC, high carrier mobility at RT and large Fermi wavelength [11]. These properties constitute Bi films as possible candidates for electronic and spintronic applications.

Among Bi allotropes two are the most stable: the so-called hexagonal Bi (111) (hex) and Bi pseudocubic (110) (PC) phases [12- 14]. The hexagonal (111) structure on the distorted A7 phase, is the honeycomb hexagonal lattice of Bi and exists as a single bilayer [12-17]. The successful experimental growth of a hexagonal single bilayer Bi honeycomb lattice (i.e bismuthene) has been reported and a large band-gap 2D TI behavior has been assigned to this material [18]. Bi(111) bilayer has also been studied on Bi_2Te_3 [19, 20]. Overall it turns out that Bi(111) exhibits

topological non-trivial behavior independently of the number of layers.

On the other hand, the PC-Bi on the so-called distorted A17 phase adopts the black phosphorous like (BP-like) structure and crystallizes in a rectangular unit cell consisting of two paired layers with an atom near the middle of the unit cell [12-15, 21, 22] Contrary to the hex-phase, the topological properties of the Bi(110) edge states depend on in-plane or out-of plane strains [22] and therefore on the interactions between the Bi films and the substrates.

It has been shown both theoretically and experimentally that the PC phase transforms into the hex Bi phase above a critical thickness [21-22]. When grown on a Si substrate Bi(110) is stable up to 4 ML (2BL), whereas a critical thickness up to 60 ML is observed in the case of an Au substrate [23].

Both Bi(111) and Bi(110) structures are of high importance because their edges may support topologically protected edge states [12, 24].

The "fusion" between non-trivial topological order and 2D crystals could radically change nanoelectronics bringing spin into play in very unique ways, paving the way to a revolutionary exploitation of dissipation-less spin channels for both electronics and spintronics.

In this work, we grew ultrathin Bi films on InAs(111)/$HfTe_2$ templates by molecular beam epitaxy (MBE), and measured the atomic and electronic structures by *in-situ* Reflection High Energy Electron Diffraction (RHEED), X-ray Photoelectron Spectroscopy (XPS), Angle-Resolved Photoemission Spectroscopy (ARPES), Scanning Tunneling Microscopy (STM) and Raman techniques. High quality epitaxial growth is expected for Bi on top of the 2D-$HfTe_2$ substrate, in agreement with the van der Waals heteroepitaxial nature of $HfTe_2$ material [25].

2. Experimental

Thin Bi films were prepared by MBE in an ultrahigh-vacuum (UHV) chamber at RT. High-purity Bi (99.999%) was evaporated by Knudsen cells with deposition rate of ~0.1 Å /min. Prior to Bi growth, Si(111)/InAs(111) substrates were cleaned according to the procedure described in detail in Ref. [26], whereas thin (2 ML) $HfTe_2$ semimetallic films were deposited at 400 °C as a template [25]. In situ lab-based ARPES measurements were performed using a SPECS PHOIBOS 100 hemispherical analyzer equipped with a 2D CCD detector and He I radiation at 21.22 eV, with total energy resolution of 100meV (due to thermal broadening at RT). In situ X-ray photoelectron spectroscopy (XPS) was performed with excitation by Mg Kα radiation (1253.6 eV) using a SPECS XR50 source, at a take-off angle of 52°. In-situ STM measurements were carried out at RT, with an Omicron LS–STM using a Pt-Ir tip. STM images processing was made by SPIP program. For ex-situ measurements, Bi on $HfTe_2$ was a capped by 2.5 nm of amorphous Al_2O_3 layer. Ex-situ Raman spectroscopy was performed with a Renishaw InVia Raman microscope equipped with 514 nm Ar + laser. The first-principles calculations were performed using the Vienna Ab Initio Simulation Package [27,28] and projector augmented waves [29]. The generalized-gradient approximation with Perdew-Burke-Ernzerhof [30] parametrization was used as the exchange correlation functional. The kinetic energy cutoff was set at 500 eV, using the Monkhorst-Pack scheme [31] employing a 9 × 9 × 1 k-point mesh. Also, a vacuum 15Å was used to avoid interaction between the periodically repeated layers. The atomic positions were fully optimized by conjugate gradient, using a force threshold of 10^{-3}eVÅ^{-1}. Spin-orbit coupling was included in band structure calculations.

3. Results and Discussion

3.1 Structural Characterization

Reflection high energy electron diffraction (RHEED) patterns for the InAs/$HfTe_2$ template and the Bi epilayer are given in Fig. 1. For 6.5 Å deposition, dotted streaks are observed along both InAs azimuths (Fig. 1 c, g). These streaks are attributed to the formation of a rectangular unit cell of Bi(110) rotated 45˚ with respect to the underlying hexagonal unit cell of $HfTe_2$. The Bi(110) have the Black Phosphorus like (BP-like) A17 structure that exists in paired layer form (BL) with thickness of 1 BL $h_{Bi(110)}$~6.56 Å.

In this paper we adopt the nomenclate of S. Yaginuma et al. [15] and J. T. Sadowski et al. [32] where the 4MLs/or 2BLs of BP-like pseudocubic (PC) correspond to 13.1 Å height and the 3BLs of hexagonal Bi structures correspond to 11.8 Å (height of 1BL Bi(111)~3.93Å), as shown in Fig.2. Thus, thickness of 6.5 Å corresponds to 1BL Bi(110) [Figure 2]. Using the $HfTe_2$ RHEED pattern as reference and knowing that the lattice constant of hexagonal epitaxial $HfTe_2$ is 4.0 Å [25], the lattice constant of the tetragonal Bi(110) is estimated to 4.58 Å which is very close to the reported value of the PC Bi(110) paired layer structure [12-14].

Additional faint streaks are shown for 6.5 Å of Bi (Fig. 1c), that indicate also, the presence of the hexagonal Bi(111) phase. Upon extra deposition of Bi, at total thickness of 12 Å, the Bi(111) phase dominates with intense streaks in RHEED and the Bi(110) streaks faint away (Fig. 1d, h).

The lattice constant of hexagonal Bi(111) on $HfTe_2$ template was found 4.55Å in good agreement with the lattice reported for thicker Bi(111) films on Si(111)-(7x7) [12-14]. The thickness of 12 Å corresponds to 3 BLs of Bi(111) which is also verified by STM measurements (Fig.3).

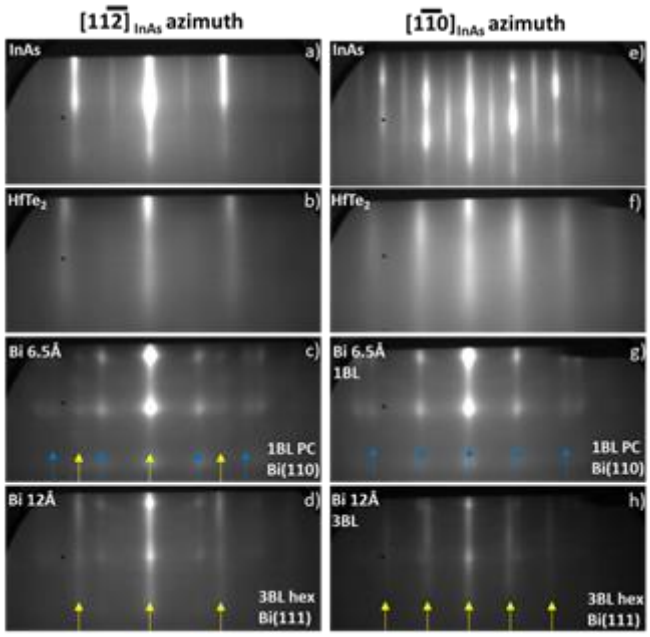

Figure 1. RHEED pattern of Bi deposition on InAs/HfTe2 templates. (a, e) Two different azimuths of (a, e) InAs(111) substrate and (b, f) 2 ML HfTe2 on InAs(111) are shown for comparison. (c, g) 6.5 Å of Bi deposited on HfTe2 and (d, h) 12 Å of Bi deposited on HfTe2. Bleu arrows indicate the main streaks of Bi(110) with tetragonal symmetry and the yellow arrows show the Bi(111) streaks with hexagonal symmetry.

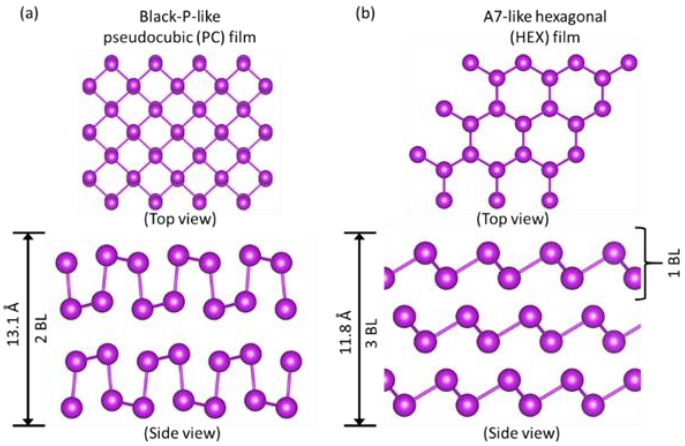

Figure 2. Schematic illustration of: a) Black-Phosphorus like pseudocubic Bi structure (α-Bi phase), where the 2BL BP-Bi correspond to 13.1 Å height (b) hexagonal Bi structure (β-Bi phase) where the 3BL Bi(111) correspond to 11.8 Å height.

In-situ room temperature STM measurements were carried out to the grown Bi films on $HfTe_2$ as shown in Fig. 3. At 6.5 Å of Bi deposition (Fig. 3a) atomically flat Bi islands with triangular and rectangular shape are formed. The large triangular areas consist of 2 layers with a step of ~0.4 nm (line profiles A and B) while the respective atomic resolution STM image indicate the hexagonal β-Bi phase (Fig. 3b). At the rectangular islands, the step height is 0.67 nm (line profile C) which corresponds to one layer of α-Bi. The atomic resolution images on the rectangular islands indicate the presence of both the BP-distorted α-Bi and the BP α-Bi phases (Fig. 3b). According to the literature [12, 17, 22] the BP-distorted α-Bi is the most common tetragonal phase where the top two Bi atoms present a bucking >0.1 Å with trivial topological properties. On the other hand, in the BP α-Bi phase the top two Bi atoms have bucking < 0.1 Å and present non-trivial topological properties [22]. Upon increasing the Bi thickness, at 12Å (Fig. 3c), the film morphology becomes very smooth and the film transforms to the hexagonal β-Bi phase (verified also by RHEED). The line profile D corresponds to 3 Bi layers with total thickness of ~11.8 Å. Therefore, the hexagonal Bi(111) film is successfully formed at 3BLs Bi film on 2D $HfTe_2$ template.

3.2 Electronic Band structure

The Bi electronic band structure of (1-2) BL (6.5Å) & 3BL (12Å) Bi films on HfTe2 template was imaged by in-situ ARPES (He I) at RT. The energy dispersion diagrams are along Γ-K-M direction of Bi(111). For (1-2) BL Bi (Fig. 4b) due to the low Bi thickness HfTe2 bands are shown around Γ-point at EBinding~0.5 eV and higher and in the region of kx~(1.2-1.5 Å-1) for E¬binding~1eV and higher. The unresolved signal at k~1Å is attributed to pseudocubic phase [14] while the bands near Fermi level at Γ and near M-point of Bi(111) are Bi(111) bands. Thus, the Fermi surface of 6.5 Å film is similar to that of pure hexagonal Bi (Fig.4a), although the respective RHEED data show mainly pseudocubic phase streaks with faint hexagonal. ARPES data of 6.5 Å film verified the findings of RHEED and STM, where the pseudocubic and hexagonal phases co-exist in the first stages of Bi growth. At 3BLs (12Å), the Fermi surface (Fig.4c) and the band structure (Fig. 4d) is clearly of Bi(111) phase in accordance to the structural RHEED and STM measurements, indicating the transition to pure hexagonal Bi. In addition, the electronic band structure of 3 BLs free standing Bi(111) calculated by DFT along the K-Γ-K direction of the Brillouin zone (BZ) shows a very good agreement with the measured ARPES data of 3BLs Bi(111) (12 Å) on HfTe2, as presented in (Fig. 4f). In case of increased number of Bi(111) layers, DFT calculations result in additional bands in the region below Γ-point, that are not observed in our experimental data

.

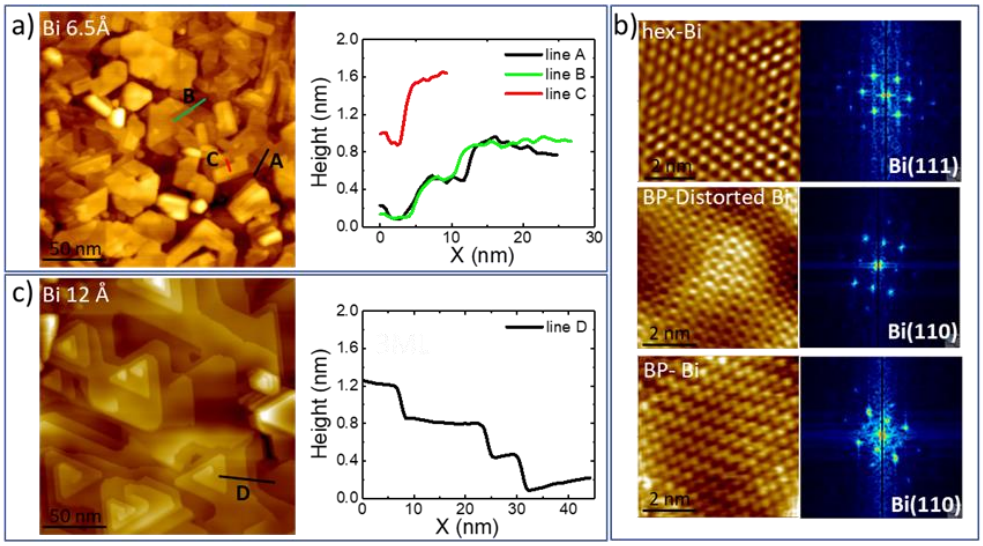

Figure. 3 STM images of Bi films grown on 2 ML $HfTe_2$ on InAs(111) at RT. (a) (200x200)nm^2 topography of 6.5 Å Bi. The Bi phases Bi(110) and Bi(111) are both present. The elongated islands are characteristic of Bi(110) while the trigonal islands are due to Bi(111). The line profiles A and B are along 2ML of Bi(111) while line profile C is along 1ML Bi(110), (b) atomic resolution images from different areas of 6.5 Å Bi film, showing the co-existence of β-Bi hexagonal, α-Bi distorted BP and α-Bi BP phases. The FFT images shows the respective hexagonal and tetragonal unit cells. c) (200x200) nm^2 topography of 12 Å Bi. The line profile D shows the formation of 3 hexagonal β-Bi layers with total height ~11.8 Å.

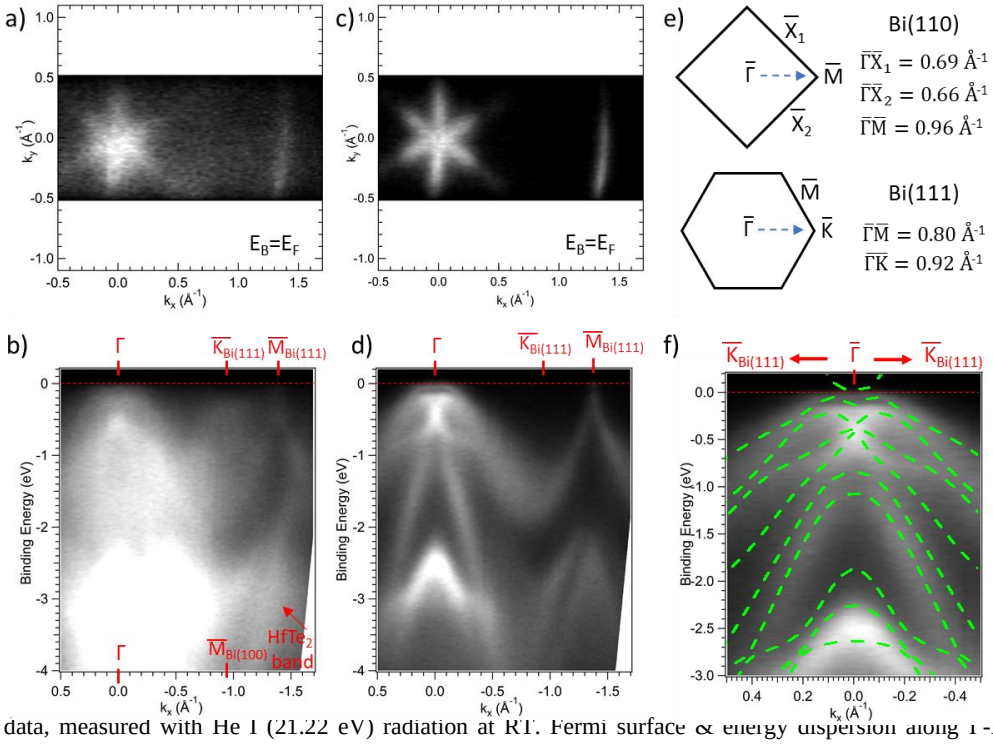

Figure 4. ARPES data, measured with He I (21.22 eV) radiation at RT. Fermi surface & energy dispersion along Γ-K-M direction of Bi(111) for: (a, b) Bi mixed (6.5 Å) PC-hexagonal phase and (c, d) 3BL Bi(111) (12 Å), respectively. (e) Surface Brillouin zone of PC and hexagonal structures, (f) Calculated band structure of 3 BL free standing Bi(111) overlaid on measured ARPES data of 3BL Bi(111) (12 Å) showing very good agreement.

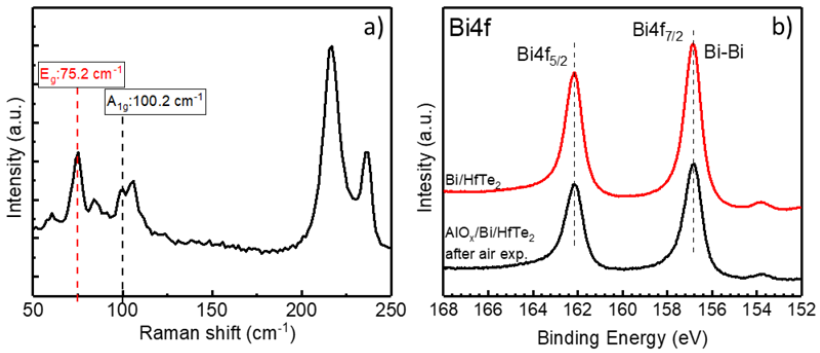

Figure 5. (a) Raman spectrum of Al_2O_3 capped 3BLs Bi(111) on $HfTe_2$/InAs after exposure to ambient conditions. The characteristic E_g and A_{1g} modes of Bi(111) are present at 75.2cm^{-1} and 100.2 cm^{-1}, respectively. The small peak at 105.5 cm^{-1} and the peaks at (200-250) cm^{-1} are from InAs/Si(111) substrate. b) XPS spectrum of Bi4f core levels of 3BLs Bi on $HfTe_2$ before air exposure and 3BLs Bi on $HfTe_2$ capped with Al_2O_3 after one-week exposure to ambient conditions. The intensity of uncapped spectrum was divided by a factor of 3 for comparison reasons. Bi peaks did not show any shift after Al_2O_3 capping and air exposure.

In the literature, the most studied case of epitaxial Bismuth growth is that of Bi on Si(111)-7x7 substrate, where the PC Bi phase is more stable than the hexagonal Bi phase for thickness <4BLs, while the a critical thickness for the transformation from tetragonal to pure hexagonal phase occurs above 6 BLs of Bi [14, 19]. The photoemission studies on Si(111)–(7x7) [14] demonstrated the coexistence of PC and hexagonal Bi over a wide range of film thicknesses. In particular, it has been shown that the two phases have different topologies. The PC phase exhibits a surface band at Γ near the Fermi level, whereas the hexagonal phase shows a Dirac-like sub-band around M. The critical thickness for the transformation from tetragonal to pure hexagonal phase occurs above 6 BLs of Bi. Here, for Bi growth on 2D HfTe2 template the transformation to pure hexagonal Bi(111) phase occurs at 12Å thickness resulting in 3 BLs Bi(111)film.

3.3 Protective capping for ambient exposure

At the low limit of atomic layers number of Xenes, such as silicene, germanene, stanene and bismuthene, the films need to be protected from possible destructive reactivity under ambient conditions. The protective layer is mandatory for the incorporation of Xenes films in a device configuration for exploiting the devices electrical performance or other applications. The in situ growth of amorphous Al_2O_3 was successfully used in the past to encapsulate silicene on Ag(111) [33] and germanene on AlN/Ag(111) [6]. Under that framework, the 3 BLs of hexagonal Bi on $HfTe_2$ films, where capped by 2.5 nm Al_2O_3 with MBE growth of Al in an oxygen overpressure of 10^{-5} mbar. The chemical stability of bismuthene layers, was assessed by ex-situ Raman (Fig. 5a) and also by XPS measurements (Fig. 5b) after one-week exposure in ambient air. In the Raman spectrum, the characteristic E_g and A_{1g} modes of Bi are present at 75.2cm^{-1} and 100.2 cm^{-1}, respectively [34, 35], while the peak at ~105.5 cm^{-1} match in plane mode of $HfTe_2$ layers [36] and the peaks at (200-250) cm^{-1} are from the substrate. Raman modes attributed to Bi oxidation were not observed [35].

4. Conclusions

Ultrathin Bi films were epitaxial grown on top of the 2D-$HfTe_2$ template by molecular beam epitaxy. At the first stage of Bi growth, for (1-2) BL (6.5Å) atomically flat Bi islands with triangular and rectangular shapes are formed with the presence of both the BP-distorted α-Bi and the BP α-Bi phases on the rectangular islands and the hexagonal β-Bi phase on the triangular islands, respectively. The coexistence of PC Bi (100) and hexagonal Bi(111) phases for 1-2 BL of Bi is also evident in the ARPES data of the electronic band structure. The transformation to the pure hexagonal phase was already observed for the thickness of 12 Å, resulting in 3BL Bi(111) on 2D-$HfTe_2$, with the electronic band structure of 3BL Bi(111) on 2D-$HfTe_2$ in agreement with the theoretical calculations of 3 BLs free standing Bi(111). The depositing of Al_2O_3 capping layer on top of the ultrathin 3BL Bi layers, seems to prevent their oxidation, which would allow potential application of ultrathin Bi layers for electronic devices such as spintronics and energy applications.

Acknowledgements

The work is supported by the Hellenic Foundation for Research and Innovation and the General Secretariat for Research and Technology, under Grant No. 435 (2D-TOP) and the Horizon 2020 FETPROAC project SKYTOP – 824123- "Skyrmion - Topological Insulator and Weyl Semimetal Technology".

References

[1] Hasan M Z and Kane C L 2010 *Rev. Mod. Phys.* **82** 3045
[2] Surname A and Surname B 2009 *Journal Name* **23** 544
[3] Zhou D, Li H, Si N, Li H, Fuchs H, Niu T 2020 *Adv. Funct. Mater.* **31** 2006997
[4] Molle A, Goldberger J, Houssa M, Xu Y, Zhang S-C, Akinwande D 2017 *Nat. Mater.* **16**, 163
[5] Tsoutsou D, Xenogiannopoulou E, Golias E, Tsipas P, Dimoulas A 2013 *Appl. Phys. Lett.* **103** 231604
[6] D'Acapito F, Torrengo S, Xenogiannopoulou E, Tsipas P, Velasco J M, Tsoutsou D, Dimoulas A 2016 *J. Phys. Cond. Matt.* **28** 045002
[7] Zhu F F, Chen W-J, Xu Y, Gao C L, Guan D D, Liu C H, Qian D, Zhang S C, Jia J F 2015 *Nat. Mater.* **14** 1020
[8] Golias E, Krivenkov M, Varykhalov A, Sánchez-Barriga J, Rader O 2018 *Nano Lett.* **18** 6672
[9] Dimoulas A 2015 *Microel. Engin.* **131** 68
[10] Tao L, Cinquanta E, Chiappe D, Grazianetti C, Fanciulli M, Dubey M, Molle A, Akinwande D 2015 *Nature Nanotech.* **10** 227
[11] Ast C R, Hochst H 2003 *Phys. Rev.B* **67** 113102
[12] Kowalczyk P Z. Mahapatra O, Le Ster M, Brown S A, Bian G, Wang X, Chiang T C 2017 *Phys. Rev. B* **96** 205434
[13] Le Ster M, Maerkl T, Kowalczyk P J, Brown S A 2019 *Phys. Rev. B* **99** 075422
[14] Bian G, Miller T, Chiang T C 2009 *Phys. Rev. B* **80** 245407
[15] Yaginuma S, Nagaoka K, Nagao T, Bihlmayer G, Koroteev Y M, Chulkov E V, Nakayama T 2008 *J. Phys. Jpn.* **77** 014701
[16] Iwasaki H, Kikegawa T 1997 Acta Crys. B **53** 353
[17] Akturk E, Akturk O U, Ciraci S 2016 *Phys. Rev. B* **94** 014115
[18] Reis F, Li G, Dudy L, Bauernfeind M, Glass S, Hanke W, Thomale R, Schäfer J, Claessen R 2017 *Science* **357** 287
[19] Hirahara T, Bihlmayer G, Sakamoto Y, Yamada M, Miyazaki H, Kimura S I, Blügel S, Hasegawa S 2011 *Phys. Rev. Lett.* **107** 166801
[20] Yang F, Miao L, Wang Z F, Yao M Y, Zhu F F, Song Y R, Wang M X, Xu Z P, Fedorov A V, Sun Z, Zhang G B, Liu C, Liu F, Qian D, Gao C L, Jia J F 2012 *Phys. Rev. Lett.* **109** 01680
[21] Nagao T, Sadowski J T, Saito M, Yaginuma S, Fujikawa Y, Kogure T, Ohno T, Hasegawa Y, Hasegawa S, Sakurai T 2004 *Phys. Rev. Lett.* **93** 105501
[22] Lu Y, Xu W, Zeng M, Yao G, Shen L, Yang M, Luo Z, Pan F, Wu K, Das T, He P, Jiang J, Martin J, Feng Y P, Lin H, Wang X S 2015 *Nano Lett.* **15** 80
[23] Kawakami N, Lin C L, Kawahara K, Kawai M, Arafune R, Takagi N 2017 *Phys. Rev. B* **96** 205402
[24] Wada M, Murakami S, Freimuth F, Bihlmayer G 2011 *Phys. Rev. B* **83** 121310
[25] Giamini S A, Velasco J M, Tsipas P, Tsoutsou D, Renaud G Dimoulas A 2017 *2D Mater.* **4** 015001
[26] Tsipas P, Tsoutsou S, Fragkos S, Sant R, Alvarez C, Okuno H, Renaud G, Alcotte R, Baron T, Dimoulas A 2018 *ACS Nano* **12** 1696
[27] Kresse G, Furthmuller J 1996 *Comput. Mater. Sci.* **76** 3626
[28] Kresse G, Furthmüller J 1996 *Phys. Rev. B* **54**, 11169
[29] Blöchl P E 1994 *Phys. Rev. B* **50** 17953
[30] Perdew J P, Burke K, Ernzerhof M 1996 *Phys. Rev. Lett.* **77** 3865
[31] Monkhorst H, Pack J 1976 *Phys. Rev. B* **13** 5188
[32] Sadowski J T, Nagao T, Yaginuma S, Fujikawa Y, Sakurai T 2006 *J. Appl. Phys.* **99** 014904
[33] Molle A, Grazianetti C, Chiappe D, Cinquanta E, Cianci E, Tallarida G, Fanciulli M 2013 *Adv. Funct. Mater.* **23** 4340
[34] Walker E S, Na S R, Jung D, March S D, Kim J S, Trivedi T, Li W, Tao L, Lee M L, Liechti K M, Akinwande D, Bank S R 2016 *Nano Lett.* **16** 6931
[35] Trentelman K 2009 *J. Raman Spectrosc.* **40** 585
[36] Hangyo M, Nakashima S I, Mitsuishi A 1983 *Ferroelectrics* **52** 151